Metal−Metal Multiply-Bonded Complexes of Technetium. 2.[1] Preparation and Characterization of the Fully Solvated Ditechnetium Cation $[Tc_2(CH_3CN)_{10}]^{4+}$

Jeffrey C. Bryan,[2a] F. Albert Cotton,*[,2b] Lee M. Daniels,[2b] Steven C. Haefner,[2a,b] and Alfred P. Sattelberger*[,2a]

Inorganic and Structural Chemistry Group (CST-3), Chemical Science and Technology Division, Los Alamos National Laboratory, Los Alamos, New Mexico 87545, and Laboratory for Molecular Structure and Bonding, Department of Chemistry, Texas A&M University, College Station, Texas 77843

Received October 27, 1994[⊗]

Acidification of $Tc_2Cl_4(PR_3)_4$ with $HBF_4{\cdot}Et_2O$ in a mixture of acetonitrile and methylene chloride results in the formation of the metal−metal triply-bonded solvated complex $[Tc_2(CH_3CN)_{10}][BF_4]_4$ (**1**) in 80% yield. This compound may also be prepared through reduction of $[Bu_4N]_2[TcCl_6]$ with either Bu_3SnH or finely divided Zn followed by treatment with $HBF_4{\cdot}Et_2O$, but in lower yields (approximately 50%). The quadruply bonded species $Tc_2Cl_8^{2-}$ also reacts with $HBF_4{\cdot}Et_2O$ in a mixture of acetonitrile and diethyl ether under mild heating to produce small amounts of blue $[Tc_2(CH_3CN)_{10}][BF_4]_4$ (yield 14%). In addition to the formation of **1**, yellow crystals that proved to be the mononuclear Tc(III) species $[TcCl_2(CH_3CN)_4][BF_4]$ (**2**) were isolated in 34% yield from the reaction solution. The dinuclear cation $[Tc_2(CH_3CN)_{10}]^{4+}$ was crystallized as the mixed salt $[Tc_2(CH_3CN)_8(CF_3SO_3)_2](BF_4)_2{\cdot}CH_3CN$ (**1a**·CH_3CN) by addition of 8 equivs of $Tl(CF_3SO_3)$ to a CH_3CN solution of **1** followed by slow diffusion of a mixture of Et_2O and hexanes. Compound **1a**·CH_3CN crystallized in the tetragonal space group $P4_12_12$ with $a = 12.181(2)$ Å, $c = 27.385(3)$ Å, $V = 4063(1)$ Å^3 and $Z = 4$. The molecular structure of **1a** entails a staggered M_2L_8 conformation with approximate D_{4d} symmetry. The two axial positions of the dinuclear cation are occupied by $CF_3SO_3^-$ anions. The BF_4^- anions occupy general positions within the unit cell. The Tc≡Tc bond distance is 2.122(1) Å, consistent with a Tc−Tc multiple bond. Single crystal X-ray analysis of $[TcCl_2(CH_3CN)_4][BF_4]$ revealed a *trans* disposition of chloride ligands with approximate D_{4h} symmetry about the Tc atom. Crystal data for **2**: orthorhombic space group *Ibam*, with a = 6.250(1) Å, b = 12.189(2) Å, c = 20.880(5) Å, V = 1590.7(5) Å^3 and Z = 4. Nitrile complexes **1** and **2** have been fully characterized by a variety of physical and spectroscopic techniques including ^{1}H NMR, UV−vis and IR spectroscopies and cyclic voltammetry.

Introduction

Considerable attention has focused on the development of mono- and dinuclear metal−nitrile complexes as precursors for solid state materials,[3] catalysts[4] and extended polynuclear networks.[5] These efforts take advantage of the highly labile nature of the metal−nitrile bond. In such complexes, the labile nitrile groups may be easily displaced, thus making these complexes excellent precursors for both mononuclear and dinuclear species as well as polymers. Of particular interest are metal−metal-bonded nitrile complexes, since these species may be exploited as a convenient source of the M_2^{4+} core. To date, metal−metal-bonded species surrounded solely by acetonitrile ligands have been prepared for Mo,[6] Re,[7] and Rh.[8] Despite the growing number of homoleptic nitrile complexes for a variety of transition metals, there are no examples of similar compounds for technetium. Such complexes of technetium are expected to be versatile synthons in the development of low-valent technetium chemistry.

Currently, we are engaged in a comprehensive effort to explore and expand the boundaries of metal−metal multiple bond chemistry of ditechnetium. Compared to the wealth of chemistry associated with Re−Re multiply-bonded compounds, little is known about the related chemistry of its second row congener. Examples of metal−metal multiply-bonded complexes of technetium are primarily limited to those supported by halides and carboxylate ligands.[1,9] Our initial efforts in this area resulted in the synthesis of $Tc_2Cl_4(PR_3)_4$ (PR_3 = PEt_3, PPr^n_3, PMe_2Ph, and $PMePh_2$), the first phosphine complexes of technetium that exhibit metal−metal bonding.[1] As a continuation of this work, we now report the successful preparation of the first homoleptic nitrile complex of technetium $[Tc_2(CH_3CN)_{10}]^{4+}$. Herein, we describe the spectroscopic properties of $[Tc_2(CH_3CN)_{10}][BF_4]_4$ (**1**) and the crystal structure of $[Tc_2(CH_3CN)_8(CF_3SO_3)_2](BF_4)_2{\cdot}CH_3CN$ (**1a**·CH_3CN). In addition, we report the isolation and characterization of the mixed halide−

[⊗] Abstract published in *Advance ACS Abstracts*, March 1, 1995.

(1) Part 1: Burns, C. J.; Burrell, A. K.; Cotton, F. A.; Haefner, S. C.; Sattelberger, A. P. *Inorg. Chem.* **1994**, 33, 2257.
(2) (a) Los Alamos National Laboratory. (b) Texas A&M University.
(3) Shin, Y. K.; Nocera, D. G. *J. Am. Chem. Soc.* **1992**, *114*, 1264.
(4) (a) McCann, M.; Coda, E. M. G.; Maddock, K. *J. Chem. Soc., Dalton Trans.* **1994**, 1489. (b) Sen, A. *Acc. Chem. Res.* **1988**, *21*, 421. (c) Sen, A.; Lai, T.-W.; Thomas, R. R. *J. Organomet. Chem.* **1988**, *358*, 567. (d) Thomas, R. R.; Chebolu, V.; Sen, A. *J. Am. Chem. Soc.* **1986**, *108*, 4096.
(5) (a) Feinstein-Jaffe, I.; Barash, C. *Inorg. Chim. Acta* **1991**, *185*, 3. (b) Hoskins, B. F.; Robson, R. *J. Am. Chem. Soc.* **1990**, *112*, 1546. (c) Baxter, P.; Lehn, J.-M.; DeCain, A.; Fischer, J. *Angew. Chem., Int. Ed. Engl.* **1993**, *32*, 69.
(6) (a) Cotton, F. A.; Wiesinger, K. J. *Inorg. Chem.* **1991**, *30*, 871. (b) Cotton, F. A.; Eglin, J. L.; Wiesinger, K. J. *Inorg. Chim. Acta* **1992**, *195*, 11. (c) Mayer, J. M.; Abbott, E. H. *Inorg. Chem.* **1983**, *22*, 2774.
(7) (a) Bernstein, S. N.; Dunbar, K. R. Angew. *Chem., Int. Ed. Engl.* **1992**, *31*, 1360. (b) Bartley, S. L.; Bernstein, S. N.; Dunbar, K. R. *Inorg. Chim. Acta* **1993**, *213*, 213.
(8) (a) Dunbar, K. R. *J. Am. Chem. Soc.* **1988**, *110*, 8247. (b) Dikareva, L. M.; Andrianov, V. I.; Zhilyaev, A. N.; Baranovskii, I. B. *Russ. J. Inorg. Chem.* **1989**, *34*, 240. (c) Baranovskii, I. B.; Golubnichaya, M. A.; Zhilyaev, A. N.; Shchelokev, R. N. *Sov. J. Coord. Chem.* **1988**, 369.
(9) Cotton, F. A.; Walton, R. A. *Multiple Bonds Between Metal Atoms*, 2nd ed.; Oxford University Press: New York, 1993 and references therein.

0020-1669/95/1334-1875$09.00/0

nitrile Tc(III) complex $[TcCl_2(CH_3CN)_4][BF_4]$ (**2**) formed in the reaction of $[Tc_2Cl_8]^{2-}$ with HBF_4 in acetonitrile.

Experimental Section

General Considerations. *Caution!* The isotope ^{99}Tc is a low-energy β-emitter (E_{max} = 0.292 MeV) with a half-life of 2.12×10^5 years. All manipulations were carried out in laboratories approved for low-level radioactive materials following procedures and techniques described elsewhere.[10] Ammonium pertechnetate was obtained from Oak Ridge National Laboratory and was purified as described previously.[11] The technetium complexes $[n\text{-}Bu_4N][TcCl_6]$,[12] $[n\text{-}Bu_4N]_2[Tc_2Cl_8]$,[13] and $Tc_2Cl_4(PEt_3)_4$[1] were prepared following literature procedures. Reagents were purchased from commercial sources and used without further purification. Toluene, hexanes, THF, and diethyl ether were distilled under N_2 from either sodium or sodium/potassium alloy. Acetonitrile and methylene chloride were distilled under N_2 from CaH_2 and phosphorus pentoxide, respectively.

Synthetic Procedures. Unless noted otherwise, the transfer of air-sensitive solids and the workup of air-sensitive reaction mixtures were carried out within the confines of a Vacuum Atmospheres Co. glove box equipped with a high-capacity purification system (MO-40-2H) and a Dri-Cold freezer maintained at −40 °C.

$[Tc_2(CH_3CN)_{10}][BF_4]_4$ (1). (a) From $Tc_2Cl_4(PEt_3)_4$. To a solution of $Tc_2Cl_4(PEt_3)_4$ (0.100 g, 0.12 mmol) in a mixture of acetonitrile (1 mL) and methylene chloride (4 mL), approximately 0.5 mL of HBF_4·Et_2O (85% in diethyl ether) was added, immediately producing a blue-green solution. A slight vacuum was applied periodically to help remove any liberated HCl(g). After being stirred for 15 min at room temperature, the reaction was heated at 50 °C for 12 h. During this period, a fine blue precipitate was formed. After cooling of the solution to −40 °C, the blue solid was filtered off and washed repeatedly with diethyl ether. Pure product was obtained by slow addition of diethyl ether into an acetonitrile solution. Yield: 0.098 g (81%). ^1H NMR (CD_3CN): δ 2.95 (s, equatorial CH_3CN), 1.95 (s, free CH_3CN). Electronic absorption spectrum (CH_3CN): λ_{max}, nm (ϵ, M^{-1} cm^{-1}) 616 nm (120), 312 nm (360), 260 nm (1500) Anal. Calcd for $C_{22}H_{33}N_{11}B_4F_{16}Tc_2$:[14] C, 26.56; H, 3.34; N, 15.49. Found: C, 26.18; H, 3.30; N, 15.24. Compound **1** was also prepared in a similar manner using $Tc_2Cl_4(PMe_2Ph)_4$ and $Tc_2Cl_4(PMePh_2)_4$.

(b) From $[n\text{-}Bu_4N]_2[TcCl_6]$. Method 1. An amount of $[n\text{-}Bu_4N]_2[TcCl_6]$ (0.300 g, 0.38 mmol) was suspended in 3 mL of toluene. The suspension was heated to approximately 50 °C, and 5 equivs of $n\text{-}Bu_3SnH$ (0.4 mL, 1.9 mmol) was added dropwise by syringe. The solution became slightly colored, and an oily film appeared on the side of the reaction vessel. The toluene solution was decanted while hot, and the remaining brown residue was washed with 3 × 3 mL of toluene and 2 × 3 mL of diethyl ether. The oily solid was dried under vacuum for 1 h and then redissolved in a 5:1 mixture of CH_2Cl_2 and CH_3CN. About 0.5 mL of HBF_4·Et_2O (85% in Et_2O) was added to the solution, and a slight vacuum was applied periodically to help remove any liberated HCl(g). Over a period of 3 h, a fine blue solid separated from the blue/green solution. The solid was filtered off and washed repeatedly with methylene chloride and diethyl ether. $[Tc_2(CH_3CN)_{10}][BF_4]_4$ was recrystallized by dissolution in a minimal amount of CH_3CN followed by dropwise addition of Et_2O. After cooling of the mixture to −40 °C, the resulting blue solid was filtered off, washed with diethyl ether and dried *in vacuo*. Yield: 0.098 g (54%)

Method 2. An amount of $[n\text{-}Bu_4N]_2[TcCl_6]$ (0.050 g, 0.063 mmol) was dissolved in 3 mL of acetonitrile, and 1 equiv of finely divided zinc was added. The reaction mixture was heated to reflux. During 15 min the solution became olive and then eventually dark brown in color. After 2 h of heating, the brown solution was concentrated to approximately 1 mL and Et_2O was added until the brown product had precipitated completely from solution. The solvent was decanted, and the remaining brown solid was washed repeatedly with Et_2O. The solid was then redissolved in a 5:1 mixture of CH_2Cl_2 and CH_3CN to which about 0.5 mL of HBF_4·Et_2O (85% in Et_2O) was added. Upon addition of the acid, the solution became green and a slight vacuum was applied periodically to help remove HCl(g). Over a period of 2 h, a fine blue solid separated from solution. The solid was filtered off and washed with copious amounts of methylene chloride and diethyl ether. The compound was recrystallized as described in method 1. Yield: 0.016 g (53%).

(c) From $[n\text{-}Bu_4N]_2[Tc_2Cl_8]$. An amount of $[n\text{-}Bu_4N]_2[Tc_2Cl_8]$ (0.100 g, 0.10 mmol) was suspended in a mixture of acetonitrile (1 mL) and diethyl ether (5 mL). A quantity of HBF_4·Et_2O (0.5 mL, 85% in Et_2O) was syringed into the suspension, resulting in the immediate formation of a yellow solution and a dark brown solid. The reaction mixture was heated to 50−60 °C with an oil bath. After 1 week of heating, without stirring, the solution had become olive green and a small crop of yellow crystals had deposited at the bottom of the flask. The solution was decanted, and the crystals were saved (see below). Addition of CH_2Cl_2 to the olive solution followed by cooling overnight to −40 °C gave a blue solid. The solid was recrystallized by dissolution in a minimal amount of acetonitrile followed by slow diffusion of a layer of diethyl ether. The remaining solvent was decanted off, and the blue crystalline product was washed with diethyl ether and dried under vacuum. The product was identified as $[Tc_2(CH_3CN)_{10}][BF_4]_4$ (**1**) by spectral comparison with an authentic sample of **1** prepared as described in method 1; yield 0.014 g (14%).

$[Tc_2(CH_3CN)_8(CF_3SO_3)_2](BF_4)_2$·$CH_3CN$ (1a·CH_3CN). This compound was prepared by addition of 8 equivs of $Tl(O_3SCF_3)$ to a solution of **1** in acetonitrile. The blue solution was stirred for 15 min at room temperature and then filtered. The solution was then concentrated and transferred to a glass pipet that had been sealed at one end. The blue acetonitrile solution was carefully layered with a small amount of hexanes and finally with Et_2O.[15] The pipet was kept covered with foil. Slow diffusion of Et_2O into the CH_3CN solution resulted in the formation of large blue crystals.

$[TcCl_2(CH_3CN)_4][BF_4]$ (2). The yellow crystalline solid described in section c was washed repeatedly with CH_2Cl_2 and dried under vacuum; yield 0.030 g (34%). ^1H NMR (CD_3CN): δ 1.93 (s, free CH_3CN). Electronic absorption spectrum (CH_3CN): λ_{max}, nm (ϵ, M^{-1} cm^{-1}) 360 nm (497), 315 nm (>4000), 230 nm (>4000). Anal. Calcd for $C_8H_{12}N_4BF_4Cl_2Tc$: C, 22.88; H, 2.88; N, 13.34. Found: C, 22.81; H, 2.59; N, 13.17.

Physical Measurements. ^1H NMR spectral measurements were obtained on a Bruker WM-300 spectrometer operating at 300 MHz. ^1H chemical shifts are referenced to the residual proton impurity in the deuterated solvent. Electronic absorption spectra were measured on either a Hewlett-Packard 8450A spectrophotometer or a Perkin-Elmer 19 UV/IR/near-Ir spectrophotometer. Electrochemical measurements were performed on an EG&G Princeton Applied Research Model 273 potentiostat. Cyclic voltammetry experiments were carried out at room temperature in CH_3CN using 0.1 M $[n\text{-}Bu_4N][BF_4]$ as a supporting electrolyte. A platinum disk working electrode and a platinum wire counter electrode were used in conjunction with a silver wire quasi-reference electrode that was separated from the bulk solution by a fine porosity glass frit. $E_{1/2}$ values, determined as $(E_{p,a} + E_{p,c})/2$, are reported relative to an internal ferrocene standard. Elemental analyses were obtained on a Perkin-Elmer 2400 analyzer.

X-ray Crystallographic Procedures. Crystallographic data for $[Tc_2(CH_3CN)_8(CF_3SO_3)_2](BF_4)_2$·$CH_3CN$ (**1a**·CH_3CN) were collected using an area detector. The specific procedures used were adapted in part from those described by Scheidt[16] and are presented below. Crystallographic data for $[TcCl_2(CH_3CN)_4][BF_4]$ (**2**) were obtained using

(10) Bryan, J. C.; Burrell, A. K.; Miller, M. M.; Smith, W. H.; Burns, C. J.; Sattelberger, A. P. *Polyhedron.* **1993**, *12*, 1769 and references therein.
(11) Libson, K.; Barnett, B. L.; Deutsch, E. *Inorg. Chem.* **1983**, *22*, 1695.
(12) Nelson, C. M.; Boyd, G. E.; Smith, W. T., Jr. *J. Am. Chem. Soc.* **1954**, *76*, 348.
(13) (a) Peters, G.; Skowronek, J.; Preetz, W. *Z. Naturforsch.* **1992**, *47a*, 591. (b) Preetz, W.; Peters, G.; Bublitz, D. *J. Clust. Sci.* **1994**, *5*, 83.
(14) The crystalline product used for elemental analysis was obtained by slow diffusion of diethyl ether into an acetonitrile solution of **1** and contained an acetonitrile of crystallization.
(15) The hexanes layer, which is immiscible with acetonitrile, slows down the diffusion of diethyl ether into the acetonitrile solution.
(16) Scheidt, W. R.; Turowska-Tyrk, I. *Inorg. Chem.* **1994**, *33*, 1314.

Table 1. Crystallographic Data for $[Tc_2(CH_3CN)_8(O_3SCF_3)_2](BF_4)_2{\cdot}CH_3CN$ (**1a**·CH_3CN) and $[TcCl_2(CH_3CN)_4][BF_4]$ (**2**)

	1a·CH_3CN	**2**
formula	$C_{20}H_{27}B_2F_{14}N_9O_6S_2Tc_2$	$C_8H_{12}BCl_2F_4N_4Tc$
fw	1037.25	419.93
space group	$P4_12_12$	*Ibam*
a, Å	12.181(2)	6.250(1)
b, Å	12.181(2)	12.189(2)
c, Å	27.385(3)	20.880 (5)
V, Å^3	4063(1)	1590.7(5)
Z	4	4
ϱ_{calc}, g/cm^3	1.696	1.753
μ, cm^{-1}	8.92 (Mo Kα)	12.74 (Mo Kα)
transm coeff, max−min.		1.00−0.85
radiation (monochromated in incident beam)	Mo Kα (λ_α = 0.710 73)	Mo Kα (λ_α = 0.710 73)
temp, °C	−90 ± 2	22 ± 2
$R(F_o)^a$ ($F_o^2 > 2\sigma(F_o^2)$)	0.057	0.030
$R_w(F_o^2)^{b,c}$ (all data)	0.160	0.077
quality-of-fit-indicator^{c,d}	1.05	1.08

^{a} $R = \Sigma\,||F_o| - |F_c||\,/\Sigma|F_o|$. ^{b} $R_w = [\Sigma[w(F_o^2 - F_c^2)^2]/\Sigma[w(F_o^2)^2]]^{1/2}$. ^{c} Weight $= 1/[\sigma(F_o^2)^2 + (aP)^2 + (bP)]$, where $P = [\max(F_o^2, 0) + 2F_c^2]/3$. ^{d} Quality of fit $= [\Sigma[w(F_o^2 - F_c^2)^2]/(N_{obs} - N_{params})]^{1/2}$; based on all data.

Table 2. Atomic Coordinates and Equivalent Isotropic Displacement Parameters (Å)^2 for $[Tc_2(CH_3CN)_8(CF_3SO_3)_2](BF_4)_2{\cdot}CH_3CN$ (**1a**·CH_3CN)

	x	y	z	U(eq)^a
Tc(1)	0.8943(1)	0.0017(1)	0.0190(1)	0.029(1)
N(1)	0.7883(6)	−0.1138(6)	0.0491(2)	0.036(2)
C(1)	0.7232(8)	−0.1646(8)	0.0669(3)	0.047(2)
C(2)	0.629(1)	−0.221(1)	0.0905(4)	0.068(4)
N(2)	0.9788(5)	0.0084(6)	0.0853(2)	0.032(1)
C(3)	1.0206(7)	0.0154(7)	0.1220(3)	0.032(2)
C(4)	1.0714(9)	0.0260(9)	0.1693(3)	0.055(3)
N(3)	0.9713(6)	0.1478(6)	−0.0009(3)	0.038(2)
C(5)	1.0131(9)	0.2268(8)	−0.0112(3)	0.044(2)
C(6)	1.069(2)	0.328(1)	−0.0259(5)	0.094(5)
N(4)	0.7827(6)	0.0274(6)	−0.0364(2)	0.038(2)
C(7)	0.7124(9)	0.0573(8)	−0.0597(4)	0.047(2)
C(8)	0.623(1)	0.099(1)	−0.0908(5)	0.083(4)
S(1)	0.6618(2)	0.1338(3)	0.0752(1)	0.066(1)
O(1)	0.7751(5)	0.1300(6)	0.0603(2)	0.047(2)
O(2)	0.5903(8)	0.0583(8)	0.0508(4)	0.094(3)
O(3)	0.6487(9)	0.148(1)	0.1257(4)	0.137(6)
C(9)	0.630(2)	0.253(2)	0.0547(5)	0.125(8)
F(1)	0.635(1)	0.2733(9)	0.0074(4)	0.163(6)
F(2)	0.510(1)	0.276(1)	0.0632(6)	0.193(7)
F(3)	0.668(1)	0.3448(9)	0.0738(5)	0.149(4)
B(1)	0.166(2)	0.322(2)	0.112(1)	0.19(2)
F(4)	0.073(1)	0.364(1)	0.0941(5)	0.159(5)
F(5)	0.163(2)	0.219(2)	0.0995(8)	0.191(5)
F(6)	0.227(2)	0.348(2)	0.0665(8)	0.191(5)
F(7)	0.226(2)	0.390(2)	0.1314(7)	0.191(5)
F(8)	0.148(2)	0.287(2)	0.1633(7)	0.191(5)
N(5)	0.669(2)	0.569(2)	0.0162(7)	0.086(7)
C(10)	0.755(2)	0.529(2)	0.0220(9)	0.068(7)
C(11)	0.856(2)	0.478(3)	0.027(1)	0.09(1)

^{a} Equivalent isotropic U_{eq} is defined as one-third of the trace of the orthogonalized U_{ij} tensor. Atoms N(5), C(10), and C(11) were refined at half-occupancy. Atoms F(5)−F(8) were refined at 3/4 occupancy.

general procedures that have been fully described elsewhere.[17] All calculations were performed on a local area VMS cluster at Texas A&M University. Data were corrected for Lorentz and polarization effects. Crystallographic parameters and basic information pertaining to data collection and structure refinement are summarized in Table 1. A listing of positional and isotropic parameters for compounds **1a**·CH_3CN and **2** are presented in Tables 2 and 3, respectively. Selected bond distances and angles are listed in Tables 4 and 5. Tables of anisotropic displacement parameters as well as complete tables of bond distances and angles are available as supplementary material.

Table 3. Atomic Coordinates and Equivalent Isotropic Displacement Parameters (Å^2) for $[TcCl_2(CH_3CN)_4][BF_4]$ (**2**)^a

	x	y	z	U(eq)^a
Tc(1)	0.5	0.5	0	0.033(1)
Cl(1)	0.2839(3)	0.3447(1)	0	0.044(1)
N(1)	0.3054(7)	0.5703(3)	−0.0689(2)	0.040(1)
C(1)	0.1951(8)	0.6108(4)	−0.1046(2)	0.042(1)
C(2)	0.057(1)	0.6621(7)	−0.1506(4)	0.068(2)
B(1)	0	0	0.25	0.052(3)
F(1)	0.118(1)	0.0627(5)	0.2880(3)	0.157(3)

^{a} Equivalent isotropic U_{eq} is defined as one-third of the trace of the orthogonalized U_{ij} tensor.

Table 4. Selected Bond Lengths (Å) and Angles (deg) for $[Tc_2(CH_3CN)_8(CF_3SO_3)_2](BF_4)_2{\cdot}CH_3CN$ (**1a**·CH_3CN)^a

Tc(1)−Tc(1)′	2.122(1)	Tc(1)−N(1)	2.080(7)
Tc(1)−N(2)	2.090(7)	Tc(1)−N(3)	2.084(8)
Tc(1)−N(4)	2.062(8)	Tc(1)−O(1)	2.414(6)
N(1)−C(1)	1.12(1)	N(2)−C(3)	1.13(1)
N(3)−C(5)	1.12(1)	N(4)−C(7)	1.13(1)
C(1)−C(2)	1.48(1)	C(3)−C(4)	1.44(1)
C(5)−C(6)	1.47(2)	C(7)−C(8)	1.48(2)
S(1)−O(1)	1.441(7)	S(1)−C(9)	1.60(2)
S(1)−O(2)	1.431(9)	S(1)−O(3)	1.40(1)
C(9)−F(1)	1.32(2)	C(9)−F(2)	1.53(3)
C(9)−F(3)	1.32(2)		
N(1)−Tc(1)−N(2)	89.3(3)	N(1)−Tc(1)−N(3)	163.8(3)
N(1)−Tc(1)−N(4)	89.1(3)	Tc(1)′−Tc(1)−O(1)	177.7(2)
N(1)−Tc(1)−Tc(1)′	99.2(2)	N(2)−Tc(1)−Tc(1)′	98.4(2)
N(3)−Tc(1)−Tc(1)′	97.0(2)	N(4)−Tc(1)−Tc(1)′	98.0(2)
N(1)−Tc(1)−O(1)	83.0(3)	N(2)−Tc(1)−O(1)	82.2(2)
N(3)−Tc(1)−O(1)	80.8(3)	N(4)−Tc(1)−O(1)	81.4(3)
N(2)−Tc(1)−N(3)	88.4(3)	N(4)−Tc(1)−N(2)	163.5(3)
N(4)−Tc(1)−N(3)	88.6(3)	S(1)−O(1)−Tc(1)	136.9(4)
C(1)−N(1)−Tc(1)	171.1(8)	N(1)−C(1)−C(2)	173(1)
C(3)−N(2)−Tc(1)	176.6(7)	N(2)−C(3)−C(4)	178.4(9)
C(5)−N(3)−Tc(1)	179.5(7)	N(3)−C(5)−C(6)	178(1)
C(7)−N(4)−Tc(1)	164.9(8)	N(4)−C(7)−C(8)	178(1)

^{a} Symmetry transformations used to generate equiv atoms: (′) $y + 1, x - 1, -z$.

Table 5. Selected Bond Lengths (Å) and Angles (deg) for $[TcCl_2(CH_3CN)_4][BF_4]$ (**2**)^a

Tc(1)−N(1)	2.070(4)	N(1)−C(1)	1.129(6)
Tc(1)−Cl(1)	2.325(2)	C(1)−C(2)	1.435(8)
N(1)−Tc(1)−N(1)^i	91.9(2)	N(1)−Tc(1)−Cl(1)^{ii}	90.2(1)
N(1)−Tc(1)−N(1)^{ii}	180	Cl(1)−Tc(1)−Cl(1)^{ii}	180
N(1)−Tc(1)−N(1)^{iii}	88.1(2)	C(1)−N(1)−Tc(1)	177.3(4)
N(1)−Tc(1)−Cl(1)	89.8(1)	N(1)−C(1)−C(2)	179.3(6)

^{a} Symmetry transformations used to generate equiv atoms: (i) $-x + 1, -y + 1, z$; (ii) $-x + 1, -y + 1, -z$; (iii) $x, y, -z$; (iv) $x, -y, -z + 1/2$; (v) $-x, y, -z + 1/2$; (vi) $-x, -y, z$.

[$Tc_2(CH_3CN)_8(CF_3SO_3)_2$][$(BF_4)_2{\cdot}H_3CN$ (1a·CH_3CN). A crystal with the approximate dimensions 0.20 × 0.20 × 0.35 mm^3 was selected and coated with a thin layer of silicone grease. The crystal was fastened to the tip of a quartz fiber and placed in a stream of cold N_2 regulated at a temperature of −90(2) °C using an Enraf-Nonius Model FR558-S Low Temperature Controller.

Initial crystal evaluation and data collection was performed on an Enraf-Nonius FAST area detector system using the program MADNES[18] in conjunction with a 4-circle, κ-axis goniometer equipped with graphite monochromated Mo K_α radiation (λ = 0.710 73 Å). The crystal was optically centered in the X-ray beam. Because the low-temperature

(17) (a) Bino, A.; Cotton, F. A.; Fanwick, P. E. *Inorg. Chem.* **1979**, *18*, 3558. (b) Cotton, F. A.; Frenz, B. A.; Deganello, G.; Shaver, A. *J. Organomet. Chem.* **1973**, *50*, 227.

(18) Pflugrath, J.; Messerschmitt, A. MADNES, Munich Area Detector (New EEC) System, version EEC 11/9/89, with enhancements by Enraf-Nonius Corp., Delft, The Netherlands. A description of MADNES appears in: Messerschmitt, A.; Pflugrath, J. *J. Appl. Crystallogr.* **1987**, *20*, 306.

stream is collinear with the ϕ axis when χ is 0, a χ angle of 45° was used in order to position the goniometer head out of the cold stream thereby avoiding complications resulting from differential, time-dependent cooling of the goniometer head. Initial crystal evaluation typically consists of a 30−60° rotation about ω with an exposure time of 30−60 s. The image obtained upon exposure was similar to that observed for a standard rotational photograph and revealed that the crystal was suitable for further investigation.

Reflections used for unit cell determination were obtained by scanning images measured at intervals of 0.2° in a 10° range about ω. The exposure time was 10 s per image. Upon completion of the scans, ω was rotated 10° and another 10° scan was made at intervals of 0.2°. A total of six, 10° regions were scanned in the range $0 < \omega < 100°$. To enhance spectral resolution, the crystal-to-detector distance had been moved to 60 cm and the detector swing angle (θ) was set to 0. A total of 220 reflections were obtained. Fifty of these reflections were used by the auto-indexing routine ENDEX, found in the MADNES software, resulting in a preliminary primitive tetragonal unit cell. Refined cell dimensions (Table 1) were obtained by least-squares fitting of 198 reflections in the range $10 \leq 2\theta \leq 24°$. The effective mosaic spread determined by the MADNES software was 1.3° indicating that a larger scan interval should be used for data collection. As a result, the scan interval was increased to 0.3° (approximately one-third of the refined mosaicity) to account for the mosaicity of the crystal. Cell dimensions and Laue symmetry were confirmed by axial images measured using a 30° rotation about ω with an exposure time of 30 s. Data collection was performed by measuring a series of images at intervals of 0.3° about ω. The detector was set at a distance of 40 mm and a swing angle of 22.5°. These parameters work well for crystals with maximum unit cell dimensions less then 30 Å. However, for systems with longer axes the detector distance may be increased and the θ angle reduced in order to eliminate reflection overlap. Images were collected by scanning through four separate regions of space. One sweep of 110° about ω was made with $\kappa = 33°$ ($\chi = 25°$). ϕ was then rotated 90°, and a second 110° sweep of ω was made. Finally, two 75° sweeps of ω were made with $\kappa = -160°$ ($\chi = 98°$); the second sweep was made with ϕ rotated by 90° from the first. This collection procedure allows for slightly more than one hemisphere of data to be collected.[19] On the basis of the relative diffraction intensity, an exposure time of 20 s was selected. Exposure times may be varied between 3 and 40 s depending on the intensity of the diffraction pattern. Ideally, an exposure time that allows for weak high-angle data to be measured reliably, yet is short enough that the detector does not overflow when measuring intense lower angle reflections, is optimal. Images that contain reflections which overflow the detector were recollected at an attenuated detector setting. The best results are obtained when a majority of images are remeasured at the attenuated detector setting. Throughout data collection, the actual positions of reflections were compared with those predicted based on the orientation matrix. Reflections that occur outside the predicted "shoebox" region were flagged. Raw data images that were obtained were immediately evaluated using an off-line version of MADNES. The method used for evaluation involved the use of a best fit ellipsoid that gives the lowest $\sigma(I)/I$ to determine the boundaries for strong reflections. The shapes and boundaries of weak reflections are then based on those of strong reflections in the same area of the detector.[20] The data were corrected for Lorentz and polarization effects by the MADNES program. Reflection profiles were fitted, and values of F^2 and $\sigma(F^2)$ for each reflection were obtained by the program PROCOR, which uses a fitting algorithm developed by Kabsch.[21] Intensity data were examined for systematic absences by an in-house program that provides a concise listing of reflection classes to facilitate space group assignment. The reflection data file was also reformatted by the program for use with the SHELXL-93 structure refinement software package.

A total of 22 238 data were obtained in the range $4.5 \leq 2\theta \leq 56.8°$. Averaging of equiv reflections ($R_{merge} = 6.6\%$) yielded 3011 unique reflections in the range $4.5 \leq 2\theta \leq 47°$ of which 2640 were considered observed with $I > 2\sigma(I)$. The position of the metal atom was located using the direct methods program SHELXS-86. The remaining non-hydrogen atoms were located in an alternating series of least-squares cycles and difference Fourier maps. The $[BF_4]^-$ anion was found to exhibit a disorder along the B(1)−F(4) axis where the three remaining fluorine atoms were evenly distributed among 4 regions of electron density about this axis. The disorder was modeled by setting the site occupancy of the four positions (F(5), F(6), F(7), and F(8)) to $^3/_4$ and restraining their displacement parameters to be equal. The resulting model yielded reasonable bond distances and angles with respect to F(4). A molecule of CH_3CN was located in the interstices and refined at one-half occupancy, although it occupied a general position within the crystal lattice. All hydrogen atoms were included in the structure factor calculation at idealized positions and were allowed to ride on the neighboring carbon atoms. The geometric positions of the H atoms were determined by performing an initial structure factor calculation and setting the torsion angle such that the sum of electron density at the three calculated hydrogen positions of each $-CH_3$ group is maximized. Isotropic displacement parameters for the hydrogen atoms were fixed at 1.5 times that of the corresponding carbon atom. All non-hydrogen atoms were refined using anisotropic displacement parameters. Final least-squares refinement of 253 parameters resulted in residuals R (based on F) and R_w (based on F^2 for all data)[22] of 0.057 and 0.16, respectively. The quality-of-fit was 1.05 based on F^2 for all data. The absolute structure of **1a** was determined to be the correct one based on the method described by Flack (Flack x parameter = 0.07(12)).[23] A final difference Fourier map revealed that the highest remaining peak of electron density (0.89 e/Å^3) was located near Tc(1) and N(2).

$[TcCl_2(CH_3CN)_4][BF_4]$ (2). Small yellow crystals of $[TcCl_2(CH_3CN)_4][BF_4]$ (**2**) were isolated from the reaction solution as described above. A crystal with the approximate dimensions of 0.10 × 0.15 × 0.30 mm^3 was coated with a thin layer of epoxy cement and placed on the tip of a thin glass fiber. Cell parameters consistent with that of a body-centered orthorhombic lattice were obtained by least-squares refinement of 25 well-centered reflections in the range $20 < 2\theta < 35°$. The cell dimensions and symmetry were confirmed by axial photography. Data collection was performed at 20(2) °C on a Syntex P3 diffractometer equipped with graphite-monochromated Mo radiation ($\lambda_{Mo\,K\alpha} = 0.710\,73$ Å). A total of 514 data were collected in the range $3 \leq 2\theta \leq 50°$ using a $\theta-2\theta$ scan technique. Three representative reflections were measured at regular intervals and revealed that no decay in diffraction intensity had occurred. An absorption correction based on azimuthal scans of several reflections with Eulerian angle χ near 90° was applied to the data. A total of 509 data with $F_o^2 > 2\sigma(F_o^2)$ were considered observed. Examination of the systematic absences led to the selection of *Ibam* as the crystallographic space group. This choice was later confirmed by successful least-squares refinement. The atomic positions of the metal atom and the other non-hydrogen atoms were determined by heavy atom method. The positions of the hydrogen atoms were located from subsequent least-squares cycles and difference Fourier maps and were refined with isotropic thermal parameters. All non-hydrogen atoms were refined using anisotropic displacement parameters. Final least-squares refinement of 62 parameters resulted in residuals, R (based on F_o for $F_o^2 > 2\sigma(F_o^2)$) and R_w (based on F_o^2 for all data) of 0.030 and 0.077, respectively.[22] The largest remaining peak in the final Fourier difference map was 0.61 e/Å^3, and the quality-of-fit was 1.08.

(19) For triclinic crystal systems, it may be desirable to add an additional 110° sweep at $\kappa = 33°$ with ϕ rotated 180° from original sweep in order ensure that a sufficient number of Friedel opposites are measured for an accurate empirical absorption correction.

(20) (a) Lehman, M. S.; Larsen, F. K. *Acta Crystallogr., Sect. A* **1974**, *A30*, 580. (b) Wilkinson, C.; Khamis, H. W. In *Position Sensitive Detection of Thermal Neutrons*; Convert, P., Foryth, J. B., Eds.; Academic Press: New York, 1983; p 358. (c) Stansfield, R. F. D.; McIntyre, G. J. *Neutron Scattering in the Nineties*; IAEA: Vienna, 1985; p 191.

(21) (a) Kabsch, W. *J. Appl. Crystallogr.* **1988**, *21*, 67. (b) Kabsch, W. *J. Appl. Crystallogr.* **1988**, *21*, 916.

(22) R factors based on F^2 are statistically about twice as large as those based on F, and an R-index based on all data is inevitably larger than one based only on data with F greater than a given threshold.

(23) Flack, H. D. *Acta Crystallogr., Sect. A* **1983**, *A37*, 22.

Results

Synthesis. Treatment of $Tc_2Cl_4(PR_3)_4$ (PR_3 = PEt_3, PMe_2Ph, and $PMePh_2$) with an excess of $HBF_4{\cdot}Et_2O$ (>8 equiv) in a 1:5 mixture of CH_3CN and CH_2Cl_2 produces the fully solvated ditechnetium species $[Tc_2(CH_3CN)_{10}][BF_4]_4$ in high yield (eq 1). Yields up to 80% have been achieved. Although the

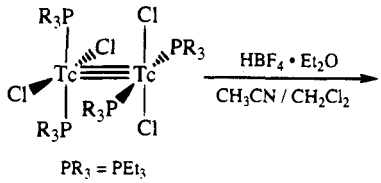

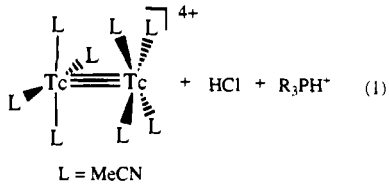

(1)

reaction does occur slowly at room temperature, heating is required to achieve maximum yields. The procedure used incorporates the methodology developed by Dunbar and coworkers to prepare the analogous dirhenium complex $[Re_2(CH_3CN)_{10}][BF_4]_4$.[7] This approach takes advantage of the strong acidity of $HBF_4{\cdot}Et_2O$ to protonate the phosphine ligands forming the corresponding phosphonium salt and to convert the chloride ions to HCl. The reaction is presumably driven both by the relative stability of the phosphonium cation which inhibits back-reaction of phosphine and the removal of volatile HCl from the reaction solution, thus effectively eliminating all other ligand sources except for the nitrile ligands which are present in large excess. Upon addition of HBF_4 to a solution of $Tc_2Cl_4(PR_3)_4$ in a 1:5 mixture of acetonitrile and methylene chloride the solution color immediately changes from purple-brown to a greenish-blue. A vacuum is applied to help remove volatile byproducts from solution. Slowly upon heating, a blue solid precipitates and is ultimately collected by filtration. The presence of CH_2Cl_2 is important to the synthesis of **1** in two respects. First, it solubilizes the dinuclear phosphine starting material. Without the addition of CH_2Cl_2, the reaction does not occur to any great extent because of the relative insolubility of $Tc_2Cl_4(PR_3)_4$ in acetonitrile. Second, the insolubility of the newly formed nitrile complex in CH_2Cl_2 causes the final product to be precipitated from solution and allows for its facile separation from the reaction byproducts. $[Tc_2(CH_3CN)_{10}][BF_4]_4$ (**1**) may be recrystallized from acetonitrile by slow addition of ether to the solution. The formation of this product does not appreciably depend on the identity of the phosphine in the complex used, since $Tc_2Cl_4(PEt_3)_4$, $Tc_2Cl_4(PMe_2Ph)_4$, and $Tc_2Cl_4(PMePh_2)_4$ all result in similar yields.

Elemental analyses performed on crystalline samples obtained from slow diffusion of hexanes and diethyl ether into acetonitrile solutions of **1** confirm the presence of the two axial nitrile ligands and allow for the formulation of the complex as $[Tc_2(CH_3CN)_{10}][BF_4]_4$ in the solid state. Compound **1** is readily soluble in acetonitrile and nitromethane but is insoluble in all other common solvents such as THF and methylene chloride. While **1** does dissolve in pyridine, the solution color changes from blue to dark red-purple and then eventually to brown, indicating that ligand substitution has occurred. Solutions and solid samples of $[Tc_2(CH_3CN)_{10}][BF_4]_4$ are unstable in air and slowly decompose upon exposure.

We have also found that $[Tc_2(CH_3CN)_{10}][BF_4]_4$ may be synthesized from higher oxidation state Tc–halide complexes. Reduction of $[Bu_4N]_2[TcCl_6]$ with either Zn or $HSnBu_3$ in hot toluene initially yields an oily brown solid. When treated with HBF_4 in a 1:5 mixture of CH_3CN and CH_2Cl_2, **1** is produced in moderate yield (eq 2). Use of either Zn or $HSnBu_3$ results in

$$[Bu_4N]_2[TcCl_6] \xrightarrow[\text{toluene, } \Delta]{2\ HSnBu_3} \text{brown solid } "[TcCl_2]_x^{n-"} \xrightarrow[CH_3CN\ /\ CH_2Cl_2]{HBF_4 \cdot Et_2O} [Tc_2(CH_3CN)_{10}][BF_4]_4 \quad (2)$$

comparable yields. Other work in this laboratory has shown that hydride reagents such as $HSnBu_3$ and $NaHBEt_3$ are excellent reagents for the reduction of metal halide species to form dinuclear and polynuclear halide clusters.[24] A slight excess of reducing agent is used to ensure complete reduction of the Tc centers to the +2 oxidation state.

Analogous to the associated dirhenium chemistry, the dinuclear complex $[n\text{-}Bu_4N]_2[Tc_2Cl_8]$ reacts with $HBF_4{\cdot}Et_2O$ under mild refluxing conditions in a mixture of CH_3CN and Et_2O to give an olive-brown solution. From this solution, $[Tc_2(CH_3CN)_{10}][BF_4]_4$ was isolated as a bright blue solid in approximately 14% yield (eq 3). Since the formation of **1** from $[Tc_2Cl_8]^{2-}$ requires a 2 electron reduction of the dimetal centers in the absence of a good reducing agent, the yield is understandably low.

$$[Bu_4N]_2[Tc_2Cl_8] \xrightarrow[CH_3CN\ /\ Et_2O,\ \Delta]{HBF_4 \cdot Et_2O} \underset{14\%}{[Tc_2(CH_3CN)_{10}][BF_4]_4} + \underset{34\%}{[TcCl_2(CH_3CN)_4][BF_4]} \quad (3)$$

In addition to the formation of **1**, the Tc(III) species $[TcCl_2(CH_3CN)_4][BF_4]$ (**2**) was isolated from the reaction solution as a yellow crystalline solid. The yield of **2** was 34% under the conditions just described. The presence of excess amounts of diethyl ether in the reaction solution plays a significant role in the isolation of **2** by precipitating the solid from the acidic medium. $[TcCl_2(CH_3CN)_4][BF_4]$ has solubility properties very similar to those described for $[Tc_2(CH_3CN)_{10}][BF_4]_4$. However, unlike **1**, solids and solutions of $[TcCl_2(CH_3CN)_4][BF_4]$ are stable in air for extended periods of time. Although the isolation of the analogous rhenium species $[ReCl_2(CH_3CN)_4][BF_4]$ has not been observed, the synthesis of several dihalide tetraamine cations of rhenium has been reported recently.[25]

Spectroscopy. The infrared spectrum of $[Tc_2(CH_3CN)_{10}][BF_4]_4$ exhibits characteristic $\nu(C{\equiv}N)$ stretching vibrations at 2330 and 2302 cm^{-1} corresponding to coordinated acetonitrile ligands. The presence of BF_4^- is readily discernible by the appearance of a strong B–F stretch near 1064 cm^{-1}. In the ^1H NMR spectrum of $[Tc_2(CH_3CN)_{10}][BF_4]_4$ in CD_3NO_2, a non-coordinating solvent, two separate resonances are observed at δ 3.00 ppm and 2.00 in a ratio of 4:1. These resonances are assigned to the equatorial and dissociated axial nitrile ligands, respectively. The ^1H NMR spectrum in CD_3CN initially shows resonances corresponding to equatorially coordinated CH_3CN at 2.95 ppm and free nitrile at 1.95 ppm. Thus, the axial CH_3CN ligands are seen to undergo immediate exchange with the deuterated solvent. As substitution of the equatorially coordi-

(24) (a) Cotton, F. A.; Daniels, L. M.; Murillo, C. A. *Inorg. Chem.* **1993**, 32, 2881. (b) Cotton, F. A.; Eglin, J. L.; James, C. A. *Inorg. Chem.* **1993**, *32*, 681. (c) Cotton, F. A.; Lu, J.; Shang, M.; Wojtczak, W. A. *J. Am. Chem. Soc.* **1994**, *116*, 4364. (d) Cotton, F. A.; Wojtczak, W. A. *Inorg. Chim. Acta* **1994**, *216*, 9. (e) Cotton, F. A.; Wojtczak, W. A. *Inorg. Chim. Acta* **1994**, *223*, 93.

(25) Orth, S. D.; Barrera, J.; Sabat, M.; Harman, W. D. *Inorg. Chem.* **1993**, *32*, 594.

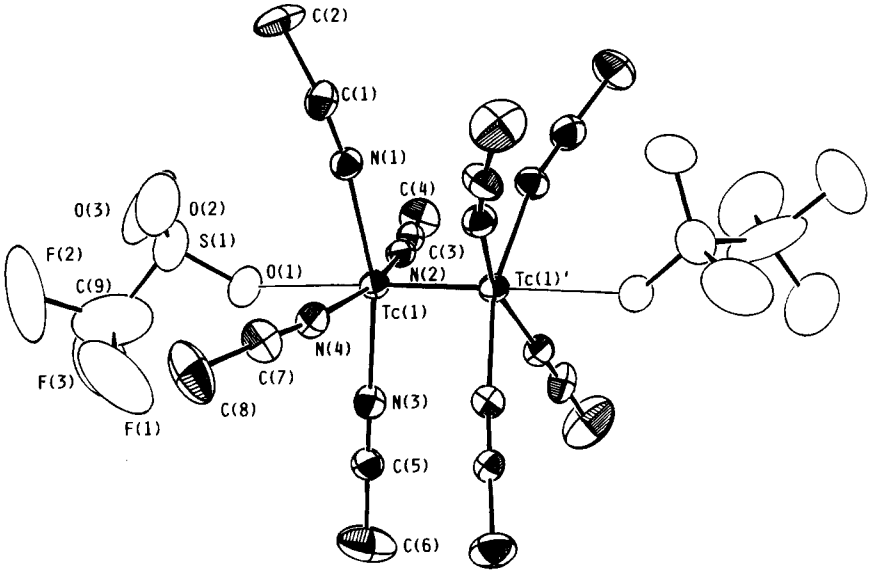

Figure 1. ORTEP drawing depicting the $[Tc_2(CH_3CN)_8(O_3SCF_3)_2]^{2+}$ cation. Thermal ellipsoids are shown at the 40% probability level.

nated CH_3CN by CD_3CN takes place the intensity of the corresponding resonance decreases until only a single resonance attributable to free nitrile is observed. The sharp and unshifted nature of the resonance of the coordinated CH_3CN molecules suggest that the molecule is diamagnetic, consistent with the presence of an electron-rich triple bond between the metal centers. The electronic spectrum of **1** in acetonitrile exhibits a broad absorption at 616 nm (120 M^{-1} cm^{-1}) which gives the complex its blue color. The low molar absorptivity of the transition is in accordance with an assignment as a metal−metal based $\delta^*-\pi^*$ transition. Higher energy absorptions are present at 312 nm (360 M^{-1} cm^{-1}) and 260 nm (1500 M^{-1} cm^{-1}).

A solid state infrared spectrum of $[TcCl_2(CH_3CN)_4][BF_4]$ shows prominent absorptions resulting from the presence of coordinated acetonitrile (ν(C≡N) = 2331, 2301 cm^{-1}) and the BF_4^- counterion (ν(B−F) = 1064 cm^{-1}). Only a single resonance attributable to free CH_3CN was observed in the ^1H NMR spectrum of **2** in CD_3CN. This demonstrates extreme lability of the coordinated nitrile ligands in this complex as well. The potential of such nitrile species as synthons for other low-valent Tc complexes is thus clear. Electronic spectroscopy indicates the presence of three transitions at 360 nm (497 M^{-1} cm^{-1}), 315 nm (>4000 M^{-1} cm^{-1}), and 230 nm (>4000 M^{-1} cm^{-1}). The latter two probably correspond to LMCT bands in view of their large extinction coefficients.

Molecular Structures. After several unsuccessful attempts at obtaining a satisfactory X-ray structure refinement of $[Tc_2(CH_3CN)_{10}][BF_4]_4$,[26] we chose to pursue a structure determination of the $[Tc_2(CH_3CN)_{10}]^{4+}$ molecular cation using other anions. Addition of 8 equivs of $Tl(O_3SCF_3)$ to an acetonitrile solution of $[Tc_2(CH_3CN)_{10}][BF_4]_4$ followed by slow diffusion of diethyl ether produced large crystals of the bis(triflate) salt $[Tc_2(CH_3CN)_8(O_3SCF_3)_2](BF_4)_2{\cdot}CH_3CN$ (**1a**·CH_3CN). An ORTEP diagram depicting the cation $[Tc_2(CH_3CN)_8(O_3SCF_3)_2]^{2+}$ is shown in Figure 1. It consists of two $Tc(CH_3CN)_4$ fragments bound by a short Tc−Tc triple bond. The pseudoplanar $Tc(CH_3CN)_4$ fragments are staggered with respect to each other (Figure 2) resulting in a torsion angle between the fragments of 43.5[1]°. Excluding the axial triflates molecules, the staggered conformation of the ML_4 fragments gives the molecular cation effective D_{4d} symmetry. The Tc−Tc bond

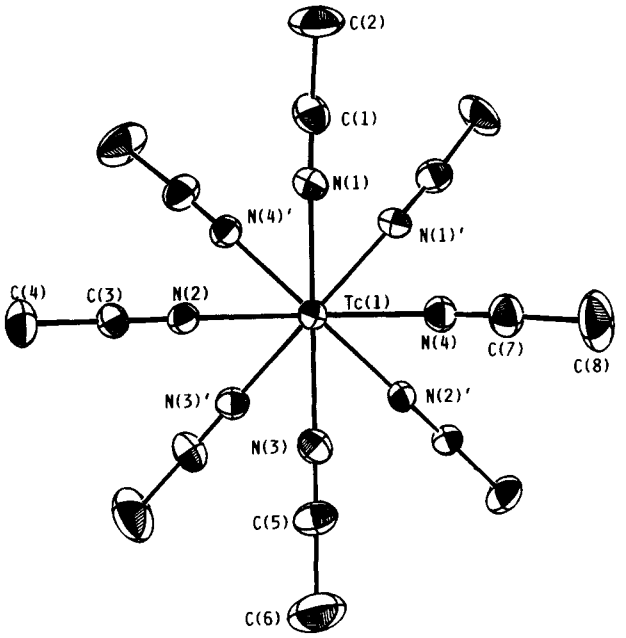

mean torsion angle = 43.5[1]°

Figure 2. $[Tc_2(CH_3CN)_8]^{4+}$ portion of the cation viewed along the Tc−Tc bond.

lies perpendicular to a 2-fold axis giving the cation crystallographically imposed C_2 symmetry. The metal−metal bond distance of 2.122(1) Å is characteristic of a multiple bond between the Tc atoms. Comparison with other technetium triply-bonded complexes shows that the Tc−Tc bond distance in **1a** is slightly shorter than those observed for $Tc_2Cl_4(PR_3)_4$ molecules (2.127(1)−2.1384(5) Å)[1] but longer than that observed in the polymeric chain complex $[Tc_2Cl_6]_n^{2n-}$ (2.044(1) Å).[27] The axial positions of the dinuclear unit are occupied by triflate anions that are weakly bonded at a distance of 2.414(6) Å. The long interaction is consistent with the weak donor ability of the triflate anion and the strong trans-effect imparted by the metal−metal multiple bond. We anticipate that, in acetonitrile, these anions are readily displaced by solvent molecules. The

(26) $[Tc_2(CH_3CN)_{10}][BF_4]_4$ crystallizes in a body-centered cubic space group with the lattice parameter a = 29.779(2) Å.

(27) (a) Cotton, F. A.; Daniels, L. M.; Falvello, L. R.; Grigoriev, M. S.; Kryuchkov, S. V. *Inorg. Chim. Acta* **1991**, *189*, 53. (b) Kryuchkov, S. V.; Grigoriev, M. S.; Kuzina, A. F.; Gulev, B. F.; Spitsyn, V. I. *Dokl. Akad. Nauk. SSR* **1986**, 389; *Engl. Transl.* **1986**, 147.

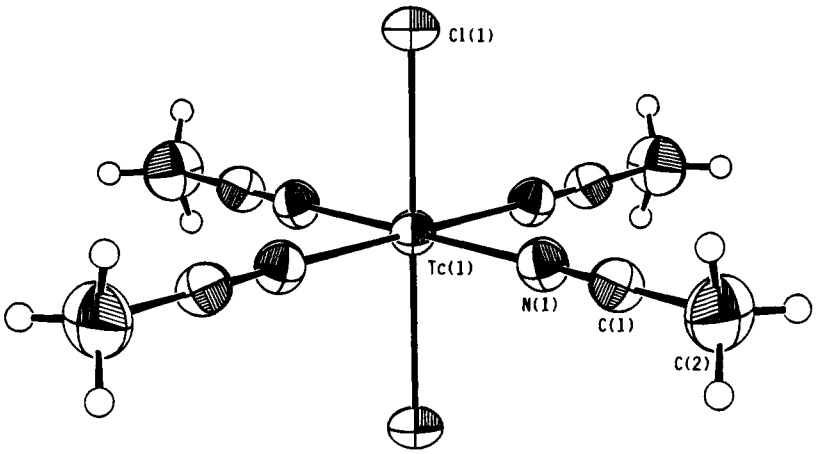

Figure 3. ORTEP diagram of the $[TcCl_2(CH_3CN)_4]^+$ cation. Thermal ellipsoids are drawn at the 40% probability level.

mean value of the Tc−N distances is within the range anticipated for such bonds. The BF_4^- anion resides on a general position within the unit cell and does not interact with the dinuclear unit.

The $[TcCl_2(CH_3CN)_4]^+$ cation, shown in Figure 3, has distorted octahedral coordination about the metal center. The chloride ligands are situated in a *trans* disposition with the nitrile ligands residing in the equatorial plane. The cation resides on a crystallographic site with *2/m* symmetry, but it has virtual D_{4h} symmetry with only a small deviation in the Cl−Tc−N bond angle from ideality (Cl−Tc−N = 90.2(1)°). Both the Tc−Cl (2.325(2) Å) and the Tc−N (2.070(4) Å) bond distances are unremarkable in that they lie in the expected ranges. The BF_4^- anions are located at van der Waals distances from the $[TcCl_2(CH_3CN)_4]^+$ and do not interact significantly with the cation.

Electrochemistry. Electrochemical studies were performed on $[Tc_2(CH_3CN)_{10}][BF_4]_4$ and $[TcCl_2(CH_3CN)_4][BF_4]$ in acetonitrile containing 0.1 M $[Bu_4N][PF_6]$ as a supporting electrolyte. A cyclic voltammogram of **1** is shown in Figure 4. It exhibits a reversible one electron reduction couple at $E_{1/2} = -0.82$ V followed by a second irreversible reduction at $E_{p,c} = -1.96$ V vs ferrocene. The second reduction has two chemical oxidation waves associated with it at $E_{p,a} = -1.06$ V and $E_{p,a} = -0.21$ V vs ferrocene. The reversibility of the first reduction couple was maintained at scan speeds ranging from 20 to 250 mV/s (Figure 4B). The reversible nature of the couple suggests that, upon addition of one electron, the metal−metal bond is retained, resulting in the formation of a stable, at least on the CV time scale, Tc(I)−Tc(II) complex. One might anticipate, that upon reduction, metal−metal bonding would be disfavored with respect to formation of a d^6, octahedral Tc(I) mononuclear species and $[Tc_2(CH_3CN)_{10}]^{4+}$. Clearly such a process does not occur during the CV experiment but may eventually occur in solution over extended periods of time. Further reduction of **1** results in a structural rearrangement as evidenced by the irreversible nature of the second reduction process. The irreversibility of this couple probably arises from complete rupture of the metal−metal bond to yield two $[Tc(CH_3CN)_6]^+$ cations. This is not surprising since promotion of a second electron into the π^* orbital might be expected to destabilize the metal−metal bond so much that formation of mononuclear d^6 species would be favored. Further studies are underway to identify products obtained upon chemical reduction of $[Tc_2(CH_3CN)_{10}]^{4+}$.

Perhaps the most surprising feature of the cyclic voltammogram of **1** is the lack of an accessible oxidation process, ubiquitous among other Tc and Re complexes which contain

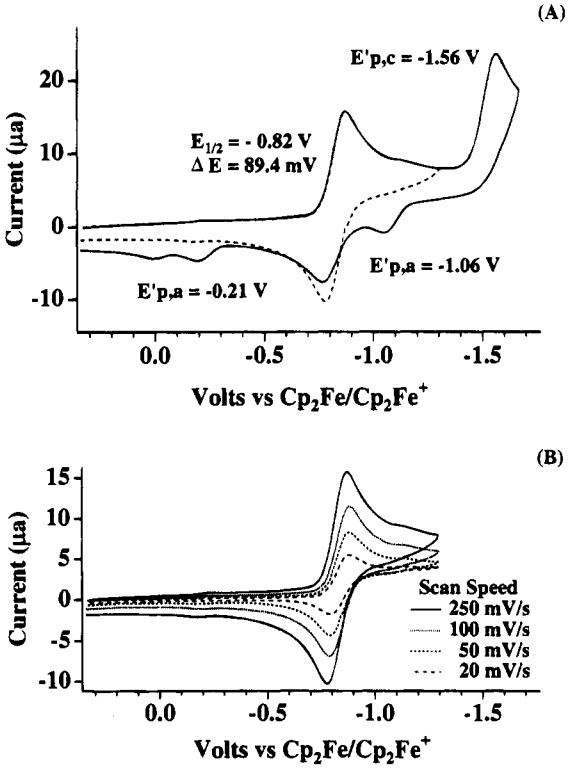

Figure 4. (A) Cyclic voltammogram of $[Tc_2(CH_3CN)_{10}][BF_4]_4$ in CH_3CN at a scan speed of 200 mV s^{-1}. (B) First reduction couple scanned at different rates.

an electron-rich triple bond.[9] The lack of an accessible oxidation process may be attributed to the high positive charge on the metal centers and the ability of nitrile ligands to stabilize low-valent metal centers. Similar behavior is common among other $[M_2(CH_3CN)_{10}]^{4+}$ species, which all readily undergo reductions but have no accessible oxidation processes.[6-8] Surprisingly, the Tc_2^{4+}/Tc_2^{3+} couple occurs at a more negative potential than that for the Re complex $[Re_2(CH_3CN)_{10}]^{4+}$ ($E_{1/2} = -0.36$ V vs ferrocene).[7] This is counterintuitive in that second row transition metals are typically more easily reduced than their third row congeners.

The cyclic voltammogram of $[TcCl_2(CH_3CN)_4][BF_4]$ shown in Figure 5 is similar to that of **1**. Complex **2** exhibits a reversible reduction at $E_{1/2} = -0.62$ V vs ferrocene. An irreversible reduction wave appears at $E_{1/2} = -1.96$ V together with a quasi-reversible chemical product couple at $E_{p,a} = -1.24$ V. The electrochemical data may be interpreted as follows: One electron reduction of $[TcCl_2(CH_3CN)_4]^+$ gives the neutral Tc(II) species $TcCl_2(CH_3CN)_4$. Upon addition of a second

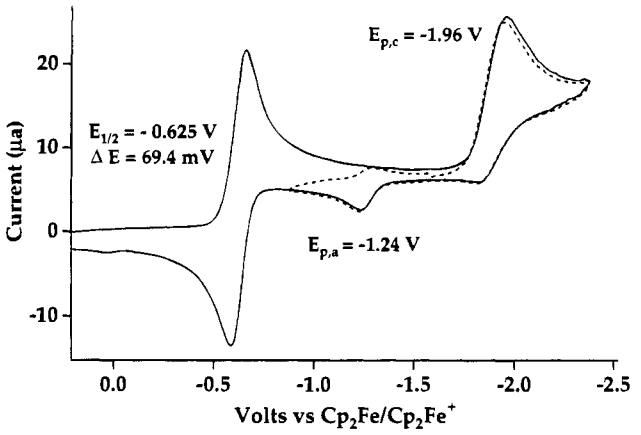

Figure 5. Cyclic voltammogram of $[TcCl_2(CH_3CN)_4][BF_4]$ in CH_3CN at a scan speed of 200 mV s^{-1}.

electron to $[TcCl_2(CH_3CN)_4]^+$, a chemical rearrangement occurs probably involving expulsion of either one or both of the chloride ligands in favor of a nitrile ligand.[28] This would effectively make the newly formed complex more difficult to oxidize, and therefore the appearance of a reversible chemical oxidation wave would occur at a more positive potential. No attempts have been made to reduce **2** chemically, but a similar Tc(II) analog, $TcCl_2(py)_4$, has been prepared by zinc reduction of $[n\text{-}Bu_4N]_2[TcCl_6]$ in pyridine.[29] Comparison of the Tc(III)/Tc(II) redox couple of **2** with that of $TcCl_2(py)_4$ ($E_{1/2}$ = −0.93 V vs ferrocene) shows that $[TcCl_2(CH_3CN)_4][BF_4]$ is reduced more readily than $[TcCl_2(py)_4]^+$. However, the Tc(III)/Tc(II) redox couple appears at more negative potentials than those of other Tc(III) dihalide and pseudohalide species supported by chelating diphosphine ligands.[11]

Discussion

The synthesis of $[Tc_2(CH_3CN)_{10}]^{4+}$ adds to the growing number of metal nitrile species that exhibit metal−metal bonding. Similar dinuclear nitrile complexes have already been prepared for Mo_2^{4+},[6] Re_2^{4+},[7] and Rh_2^{4+}.[8] Efforts are in progress in other laboratories to prepare W_2 and Os_2 analogs.[30] Synthetic strategies for the preparation dinuclear nitrile species have relied on either esterification or acidification of dimetal tetracarboxylates with trialkyloxonium salts or $HBF_4{\cdot}Et_2O$. Two of the synthetic strategies presented here were adapted from those used for the preparation of $[Re_2(CH_3CN)_{10}][BF_4]_4$, namely ligand protonation of the dinuclear species $Tc_2Cl_4(PR_3)_4$ and $[Tc_2Cl_8]^{2-}$ using $HBF_4{\cdot}Et_2O$ in acetonitrile. The third is quite different in that it uses a mononuclear precursor rather than one that already contains a metal−metal bond. The method employed involves 2 electron reduction of $[TcCl_6]^{2-}$ to produce a brown intermediate that when treated with HBF_4 in a mixture of CH_2Cl_2/CH_3CN yields $[Tc_2(CH_3CN)_{10}][BF_4]_4$. This approach is similar to a strategy used by Preetz and co-workers to prepare $[Bu_4N]_2[Tc_2Cl_8]$.[13] They reported that reduction of either $[Bu_4N]_2[TcCl_6]$ or $[Bu_4N][TcOCl_4]$ with $[Bu_4N]BH_4$ produces an oily brown intermediate that upon aerial oxidation in the presence of HCl(g) yields the quadruply bonded anion. Analogously, $[Bu_4N][TcOCl_4]$ can be used to prepare **1** but the yield is substantially lower (<10%). Although the identity of the brown intermediate is unknown, we believe that it is composed of a mixture of reduced polynuclear Tc halide species similar to those isolated upon H_2 reduction of higher-valent Tc species, e.g. $[Tc_2Cl_6]_x^{2n-}$.[31] Acidification of such clusters accompanied by removal of volatile HCl would be expected to produce the desired solvated complex. Over-reduction to form Tc(I) centers and break up of the metal−metal bonded species into mononuclear complexes during the acidification reaction probably account for the limited yields of $[Tc_2(CH_3CN)_{10}][BF_4]_4$. Although $[Tc_2(CH_3CN)_{10}][BF_4]_4$ may be obtained in greater yield from $Tc_2Cl_4(PEt_3)_4$, the overall total yield from $[TcO_4]^-$ is comparable to that using $[TcCl_6]^{2-}$ because of the number of steps involved in the preparation of $Tc_2Cl_4(PEt_3)_4$. Interestingly, zinc reduction of $TcCl_4(PPh_3)_2$ followed by treatment with HBF_4 in acetonitrile does not produce **1**. Presumably, the bulk of the PPh_3 ligands prevents formation of a dinuclear intermediate thereby thwarting the formation of $[Tc_2(CH_3CN)_{10}][BF_4]_4$.[32] Taken together, these observations suggest the importance of preformation of a metal−metal bond in order to prepare $[Tc_2(CH_3CN)_{10}][BF_4]_4$.

Both spectroscopic and structural data indicate the presence of an electron-rich triple bond between the technetium atoms. A ground state configuration of $\sigma^2\pi^4\delta^2\delta^{*2}$ electron configuration is expected on the basis of comparison with other Tc(II)−Tc(II) and Re(II)−Re(II) M_2L_8 species.[9] X-ray structural data obtained support this assertion. The staggered geometry observed for **1a** is a consequence of the absence of a net δ bond between the metal atoms. Consequently, there is no electronic barrier to rotation about the metal−metal bond and the molecule adopts the sterically favored conformation. Similar torsion angles are observed in $[Re_2(CH_3CN)_{10}][Mo_6O_{18}]_2$ and $[Rh_2(CH_3CN)_{10}][BF_4]_4$, which also lack a δ component in their bonding.[7a,8a] However, $[Mo_2(CH_3CN)_{10}][BF_4]_4$, which contains a metal−metal quadruple bond, adopts an eclipsed geometry consistent with the presence of a δ bond.[7a] Although **1a** adopts a staggered conformation in the solid state, we expect that the steric barrier to rotation is easily overcome in solution, allowing the molecule to rotate almost freely about the metal−metal bond. An elegant study of Mo and W porphyrin dimers showed that at room temperature even molecules having a δ bond have relatively unencumbered rotation in solution.[33] In the present case, rotation will be even less inhibited because of the lack of any δ component to the metal−metal bond.

Although spectroscopic and structural evidence support the presence of a electron-rich triple bond between the metal atoms, $[Tc_2(CH_3CN)_{10}][BF_4]_4$ does not exhibit the accessible oxidation process that might be expected for a species with a $\sigma^2\pi^4\delta^2\delta^{*2}$ electronic configuration. Similar redox chemistry is also displayed by other dinuclear acetonitrile cations; all $[M_2(CH_3CN)_{10}]^{4+}$ complexes readily undergo accessible reductions but do not exhibit oxidation processes. The lack of an observable oxidation process can be attributed to the high positive charge already present on the dimetal unit and the stabilizing effect of nitrile ligands on lower oxidation states.

Turning now to the mononuclear species $[TcCl_2(CH_3CN)_4]^+$ formed along with **1** in the reaction of HBF_4 with $[Bu_4N]_2[Tc_2Cl_8]$, we note that the isolation of $[TcCl_2(CH_3CN)_4][BF_4]$ raises

(28) Although this explanation appears the most plausible, we cannot rule out a *trans* to *cis* isomerization.
(29) Barrera, J.; Bryan, J. C.; Burrell, A. K. Manuscript in preparation.
(30) Bernstein, S. N.; Dunbar, K. R. 206th Presented at the American Chemical Society National Meeting, Chicago, IL, Aug 22−27, 1993; paper INOR 210.
(31) (a) Cotton, F. A.; Daniels, L. M.; Falvello, L. R.; Grigoriev, M. S.; Kryuchkov, S. V. *Inorg. Chim. Acta* **1991**, *189*, 53. (b) Kryuchkov, S. V.; Grigoriev, M. S.; Kuzina, A. F.; Gulev, B. F.; Spitsyn, V. I. *Dokl. Akad. Nauk. SSR* **1986**, 389; *Engl. Transl.* **1986**, 147.
(32) Reduction of $TcCl_4(PPh_3)_2$ in acetonitrile with 0.5 equivalents of Zn produces $TcCl_3(PPh_3)_2(CH_3CN)$ which exhibits a reversible one-electron reduction process presumably yielding $TcCl_3(PPh_3)_2(CH_3CN)^-$: Archer, C. M.; Dilworth, J. R.; Thompson, R. M.; McPartlin, M.; Povey, D. C.; Kelly, J. D. *J. Chem. Soc., Dalton Trans.* **1993**, 461.
(33) Collman, J. P.; Arnold, H. J. *J. Cluster Sci.* **1994**, *5*, 37 and references therein.

the question whether the metal−metal-bonded complex $[Tc_2Cl_4(CH_3CN)_4]^{2+}$ exists. While the preparation of the isoelectronic species $Mo_2Cl_4(CH_3CN)_4$ has been reported,[34] the analogous Tc and Re complexes are unknown. Isolation of $[TcCl_2(CH_3CN)_4]^+$ suggests that $[Tc_2Cl_4(CH_3CN)_4]^{2+}$ may be unstable with respect to metal−metal bond cleavage in acetonitrile. Unfortunately, we cannot say what role $[TcCl_2(CH_3CN)_4]^+$ might play in the formation of $[Tc_2(CH_3CN)_{10}]^{4+}$ from $[Tc_2Cl_8]^{2-}$. It seems unlikely, however, that **2** is an intermediate along the reaction pathway. It is most likely a byproduct, since for it to be an intermediate would require subsequent reduction and recombination of the metal fragments to form **1**. We offer two possible explanations for the formation of $[TcCl_2(CH_3CN)_4]^+$ from $[Tc_2Cl_8]^{2-}$. A plausible intermediate in the synthesis of **1** from $[Tc_2Cl_8]^{2-}$ is the partially solvated dinuclear species $[Tc_2Cl_4(CH_3CN)_4]^{2+}$. Treatment of $[Tc_2Cl_8]^{2-}$ with a strong acid in acetonitrile might be expected to first replace four chloride ligands by nitriles to form $[Tc_2Cl_4(CH_3CN)_4]^{2+}$ which is isoelectronic with the known compound $Mo_2Cl_4(CH_3CN)_4$.[34] This species might then undergo reduction and further halide substitution to produce $[Tc_2(CH_3CN)_{10}][BF_4]_4$. Subsequent metal−metal bond cleavage of $[Tc_2Cl_4(CH_3CN)_4]^{2+}$ in acetonitrile would then yield the observed mononuclear complex $[TcCl_2(CH_3CN)_4]^+$. Alternatively, scission of $[Tc_2Cl_8]^{2-}$ in acetonitrile would give 2 equivs of $[TcCl_4(CH_3CN)_2]^-$ that in the presence of excess HBF_4 could expel Cl^- in favor of two acetonitrile ligands. Previous work has shown that $[Re_2Cl_8]^{2-}$ undergoes photolysis in acetonitrile to yield two $[ReCl_4(CH_3CN)_2]^-$ moieties that then go on to lose a chloride ion in favor of acetonitrile and form $ReCl_3(CH_3CN)_3$.[35] In the present case, the acidic conditions may promote further substitution chemistry to produce $[TcCl_2(CH_3CN)_4]^+$. Clearly, both paths appear plausible and further work would be required to elucidate the pathway involved in the formation of $[Tc_2(CH_3CN)_{10}][BF_4]_4$ from $[Tc_2Cl_8]^{2-}$.

Acknowledgment. This work was supported by the Laboratory Directed Research and Development Program at Los Alamos National Laboratory. The authors also acknowledge financial assistance from the National Science Foundation and the Laboratory for Molecular Structure and Bonding for support of the facilities at Texas A&M University. We thank Dr. Carol Burns (Los Alamos National Laboratory) for helpful discussions. The authors also thank Dr. Robert Hightower (Oak Ridge National Laboratory) for a generous gift of ammonium pertechnetate.

Supplementary Material Available: Tables of crystallographic parameters, atomic hydrogen positional and thermal parameters, complete bond distances and angles, and anisotropic thermal parameters (13 pages). Ordering information is given on any current masthead page.

IC941240G

(34) San Filippo, J., Jr.; Sniadoch, H. J.; Grayson, R. L. *Inorg. Chem.* **1974**, *13*, 2121.

(35) Geoffroy, G. L.; Gray, H. B.; Hammond, G. S. *J. Am. Chem. Soc.* **1974**, *96*, 5565.